Electromagnetically induced grating in a thermal N-type four-level atomic system*

Ya-Bin Dong(董雅宾)†, Jun-Yan Li(李俊燕), and Zhi-Ying Zhou(周志英)

Department of Physics, Shanxi University, Taiyuan 030006, *China*

(Received 22 June 2016; revised manuscript received 2 September 2016; published online 30 November 2016)

The electromagnetically induced grating effect in thermal and cold atoms has been studied theoretically. Studies have shown that, by adjusting the parameters, the first-order diffraction efficiency of the probe beam in the cold atomic system and the thermal atomic system is 34% and 31%, respectively, which is very close to the ideal diffraction efficiency of the sinusoidal grating. However, it is more difficult to prepare the cold atomic system than to prepare the thermal atomic system in the practical application, so the study of the electromagnetically induced grating effect in the thermal atomic system may be helpful for practical applications.

Keywords: electromagnetically induced grating, phase modulation, first-order diffraction efficiency, thermal atomic system

PACS: 42.50.Gy, 42.65.An **DOI:** 10.1088/1674-1056/26/1/014202

1. Introduction

In recent years, the atomic coherence effects have aroused widespread interest. Using a standing wave to replace the traveling wave of electromagnetically induced transparency (EIT),[1,2] an electromagnetically induced grating (EIG)[3–5] is formed. It is not easy for the traditional grating to change the properties of the grating, however, the electromagnetically induced grating can through the real-time modulate signal and coupling field to change the properties of the grating in real-time, and then can real-time modulate the diffraction of the probe field, thus overcoming the limitations of the ordinary grating. Hence, it has great application prospects in all-optical switches and all-optical network control.[6,7]

In 1998, the electromagnetically induced amplitude grating in the ultracold Lambda atomic system was studied theoretically.[3] Later, the EIG phenomena in the cold atomic system were observed experimentally.[8,9] In 2005, Xiao *et al.* applied the EIG effect to an all-optical switch and routing.[6] Besides, the diffraction work of electromagnetically induced grating in photonic bandgap reflection atomic medium and atomic-like EIT medium has also been studied.[10–12]

EIG phenomena in different cold atomic systems have attracted more and more attention.[13–20] However, it is more difficult to prepare a cold atomic system than to prepare a thermal atomic system in practical applications. Based on these considerations, in this article, we theoretically studied the electromagnetically induced phase grating in both the thermal atomic system and the cold atomic system, and found that the first-order diffraction efficiency in the thermal atomic system is very close to that in the cold atomic system, so the study of EIG effect in the thermal atomic system may be of some help to practical applications.

The rest of this paper is organized as follows: in Section 2, we give the theoretical model and the equations; the results of theoretical simulation are discussed in Section 3; Section 4 gives the conclusion.

2. Model and equations

The N-type four-level atomic structure model is shown in Fig. 1. The hyperfine levels $5^2S_{1/2}$, $F = 1$ and 2 of ^{87}Rb are chosen to be $|1\rangle$ and $|2\rangle$, $5^2P_{1/2}$, $F = 1$ to be $|3\rangle$ and $5^2P_{3/2}$, $F = 2$ to be $|4\rangle$, respectively. A weak probe beam with a Rabi frequency Ω_p couples to the transitions $|1\rangle$ and $|3\rangle$, while the coupling field and signal field connection level $|2\rangle \leftrightarrow |3\rangle$ and $|2\rangle \leftrightarrow |4\rangle$ with a Rabi frequency Ω_c and Ω_s, respectively. If the signal wave is formed by two overlapping fields that form a standing wave in the x direction, the Rabi frequency of signal field can be written as $\Omega_s(x) = \Omega_s \sin(\pi x/\Lambda)$, where Λ represents the space period of a standing wave.

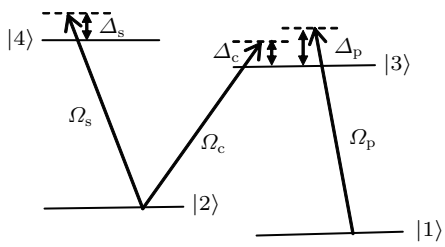


Fig. 1. The N-type four-level atomic system level structure. An N-type four-level atom interacting with three laser beams: probe (Ω_p), coupling (Ω_c), and signal (Ω_s).

*Project supported by the National Natural Science Foundation of China (Grants Nos. 11004126 and 61275212) and the Natural Science Foundation of Shanxi Province, China (Grant No. 2011021003-1).

†Corresponding author. E-mail: ybdong@sxu.edu.cn

© 2017 Chinese Physical Society and IOP Publishing Ltd

With the approximate dipole and the rotational wave approximation, the interaction Hamiltonian is given by[3]

$$\begin{aligned} H_{\rm I} = & -\hbar[\Omega_{\rm p}\,{\rm e}^{-{\rm i}\Delta_{\rm p}t+{\rm i}k_{\rm p}z}|3\rangle\langle 1| + \Omega_{\rm c}\,{\rm e}^{-{\rm i}\Delta_{\rm c}t+{\rm i}k_{\rm c}z}|3\rangle\langle 2| \\ & + \Omega_{\rm s}\sin(\pi x/\Lambda)\,{\rm e}^{-{\rm i}\Delta_{\rm s}t+{\rm i}k_{\rm s}z}|4\rangle\langle 2| + {\rm c.c.}], \end{aligned} \tag{1}$$

where

$$\Omega_{\rm p} = \frac{er_{31}E_{\rm p}}{2\hbar}, \quad \Omega_{\rm c} = \frac{er_{32}E_{\rm c}}{2\hbar}, \quad \Omega_{\rm s} = \frac{er_{42}E_{\rm s}}{2\hbar}.$$

In the thermal atomic system, we consider the influence of the atomic motion with Doppler effect. When the atom moves with a velocity of v, we define the propagation direction of the probe beam as the positive direction, the detunings are then $\Delta_{\rm p} = \omega_{\rm p} - \omega_{31} - k_{\rm p}v_z$, $\Delta_c = \omega_c - \omega_{32} - k_{\rm c}v_z$, and $\Delta_{\rm s} = \omega_{\rm s} - \omega_{42}\omega_{\rm p} - k_{\rm s}v_z$, respectively. Among them, $\omega_{\rm p}$, $\omega_{\rm c}$, and $\omega_{\rm s}$ are the circular frequencies of the probe, coupling, and signal (standing) waves, while ω_{31}, ω_{32}, and ω_{42} are the corresponding frequencies of the atomic transition. The equations of the density-matrix elements for N-type atomic system are then given by[3]

$$\begin{aligned} \frac{\partial\rho_{11}}{\partial t} &= {\rm i}\Omega_{\rm p}^*\rho_{31} - {\rm i}\Omega_{\rm p}\rho_{13} + \Gamma_{31}\rho_{33}, \\ \frac{\partial\rho_{21}}{\partial t} &= \left[-\gamma_{21} + {\rm i}\left(\Delta_{\rm p} - \Delta_{\rm c}\right)\right]\rho_{21} + {\rm i}\Omega_{\rm c}^*\rho_{31} \\ &\quad + {\rm i}\Omega_{\rm s}^*\sin(\pi x/\Lambda)\rho_{41} - {\rm i}\Omega_{\rm p}\rho_{23}, \\ \frac{\partial\rho_{31}}{\partial t} &= \left(-\gamma_{31} + {\rm i}\Delta_{\rm p}\right)\rho_{31} + {\rm i}\Omega_{\rm c}\rho_{21} + {\rm i}\Omega_{\rm p}(\rho_{11} - \rho_{33}), \\ \frac{\partial\rho_{41}}{\partial t} &= \left[-\gamma_{41} + {\rm i}(\Delta_{\rm s} + \Delta_{\rm p} - \Delta_{\rm c})\right]\rho_{41} \\ &\quad + {\rm i}\Omega_{\rm s}\sin(\pi x/\Lambda)\rho_{21} - {\rm i}\Omega_{\rm p}\rho_{43}, \\ \frac{\partial\rho_{22}}{\partial t} &= {\rm i}\Omega_{\rm c}^*\rho_{32} - {\rm i}\Omega_{\rm c}\rho_{23} + {\rm i}\Omega_{\rm s}^*\sin(\pi x/\Lambda)\rho_{42} \\ &\quad - {\rm i}\Omega_{\rm s}\sin(\pi x/\Lambda)_{24} + \Gamma_{32}\rho_{33} + \Gamma_{42}\rho_{44}, \\ \frac{\partial\rho_{32}}{\partial t} &= (-\gamma_{32} + {\rm i}\Delta_{\rm c})\rho_{32} - {\rm i}\Omega_{\rm s}\sin(\pi x/\Lambda)\rho_{34} \\ &\quad + {\rm i}\Omega_{\rm p}\rho_{12} + {\rm i}\Omega_{\rm c}(\rho_{22} - \rho_{33}), \\ \frac{\partial\rho_{42}}{\partial t} &= (-\gamma_{42} + {\rm i}\Delta_{\rm s})\rho_{42} - {\rm i}\Omega_{\rm c}\rho_{43} \\ &\quad - {\rm i}\Omega_{\rm s}\sin(\pi x/\Lambda)(\rho_{44} - \rho_{22}), \\ \frac{\partial\rho_{33}}{\partial t} &= {\rm i}\Omega_{\rm p}\rho_{13} - {\rm i}\Omega_{\rm p}^*\rho_{31} + {\rm i}\Omega_{\rm c}\rho_{23} \\ &\quad - {\rm i}\Omega_{\rm c}^*\rho_{32} - (\Gamma_{31} + \Gamma_{32})\rho_{33}, \\ \frac{\partial\rho_{43}}{\partial t} &= [-\gamma_{34} + {\rm i}(\Delta_{\rm s} - \Delta_{\rm c})]\rho_{43} + {\rm i}\Omega_{\rm s}\sin(\pi x/\Lambda)\rho_{23} \\ &\quad - {\rm i}\Omega_{\rm p}^*\rho_{41} - {\rm i}\Omega_{\rm c}^*\rho_{42}, \\ \frac{\partial\rho_{44}}{\partial t} &= {\rm i}\Omega_{\rm s}\sin(\pi x/\Lambda)\rho_{24} - {\rm i}\Omega_{\rm s}^*\sin(\pi x/\Lambda)\rho_{42} - \Gamma_{42}\rho_{44}, \\ \rho_{ji} &= (\rho_{ij})^*, \quad (i \neq j), \\ \rho_{11} &+ \rho_{22} + \rho_{33} + \rho_{44} = 1, \end{aligned} \tag{2}$$

where Γ_{ij} is the population decay rate from level i to j and γ_{ij} is the dephasing rate between the corresponding levels.

By Eq. (2), we can obtain a numerical solution of the density matrix equations. The solution contains the speed of the atoms along the z direction, so we can integrate the velocity of the atom along the z direction by using this solution, and the average density matrix element of the system is obtained. At the same time, we know that the speed of the atoms obeys the Maxwell–Boltzmann's distribution (M–B),[21] so the velocity distribution in the z direction is

$$f_v(v_z) = \sqrt{\frac{m}{2\pi kT}}\left[\frac{-mv_z^2}{2kT}\right]. \tag{3}$$

Here, k is the Boltzmann constant, m is the quality of the rubidium atoms, T is the temperature, and v_z is the speed of the atoms in the z direction.

Assume that the probe beam is spreading along the z direction through an atomic medium with a length of L. Under the slowly varying amplitude approximation, at the same time, in order to get the result of the dimensionless form, we set γ_{31} as the unit for all Rabi frequency, detuning, and the attenuation rate; Λ as the unit for x; and z_0 as the unit for z. We can then obtain propagation equations of the probe beam by Maxwell's equations[3]

$$\frac{-{\rm i}}{N_F}\frac{\partial^2\Omega_{\rm p}}{\partial x^2} + \frac{\partial\Omega_{\rm p}}{\partial z} = (\alpha_{\rm r} + {\rm i}\alpha_{\rm i})\Omega_{\rm p}, \tag{4}$$

where $\alpha_{\rm r} = -{\rm Im}\left[\rho_{31}\right]\gamma_{31}/\Omega_{\rm p}$ and $\alpha_{\rm i} = {\rm Re}\left[\rho_{31}\right]\gamma_{31}/\Omega_{\rm p}$. The $N_{\rm F} = \frac{\left(2\sqrt{\pi}\Lambda\right)^2}{\lambda_{\rm p}z_0}$ is the Fresnel number of a slit of a width $2\sqrt{\pi}\Lambda$ at a distance of z_0.

Because $\Omega_{\rm s}(x)$ is the function of x, $\alpha_{\rm r}$, and $\alpha_{\rm i}$ are also functions of x. Equation (4) can be solved analytically to obtain the transmission function of the atomic medium at $z = L$,

$$T(x) = {\rm e}^{\alpha_{\rm r}(x)L}\,{\rm e}^{{\rm i}\alpha_{\rm i}(x)L}. \tag{5}$$

By Fourier transform of $T(x)$, we can get the Fraunhofer diffraction or far-field diffraction equation [3]

$$I_{\rm p}(\theta) = \left|E_{\rm p}^1(\theta)\right|^2\frac{\sin^2\left(M\pi\Lambda\sin\theta/\lambda_{\rm p}\right)}{M^2\sin^2\left(\pi\Lambda\sin\theta/\lambda_{\rm p}\right)}, \tag{6}$$

where $E_{\rm p}^1(\theta) = \int_0^1 T(x)\exp\left(-{\rm i}2\pi\Lambda x\sin\theta/\lambda_{\rm p}\right){\rm d}x$ corresponds to the Fraunhofer diffraction of a single space period, M is the number of spatial periods of the grating illuminated by the probe light, and θ is the diffraction angle of the probe light with respect to the z direction.

3. Results and discussion

We assume $\gamma_{31} = \gamma_{32} = \gamma_{42} = \gamma$, $\gamma_{21} = \gamma_{43} = \gamma_{41} = 0.004\gamma$, and $\Gamma_{31} = \Gamma_{32} = \Gamma_{42} = 0.66\gamma$ with γ being the natural linewidth of state $|3\rangle$. Figure 2 displays the transmission function $T(x)$ as a function of x. The solid curves and dashed curves represent the results of amplitude modulation and phase modulation, respectively. As shown in Fig. 2(a), in the cold atomic system, there is a very small effect on the transfer function

which oscillates around an average transmissivity of 97.7% when only the amplitude modulation exists; however, when the phase modulation is added, a great effect on the modulation transfer function reaching the maximum phase shift value of 1.17π is observed. Similarly, as shown in Fig. 2(b), in the room-temperature atomic system, the phase modulation on the transfer function is larger than the amplitude modulation effect, which makes a great improvement in the first-order diffraction efficiency of the probe beam.

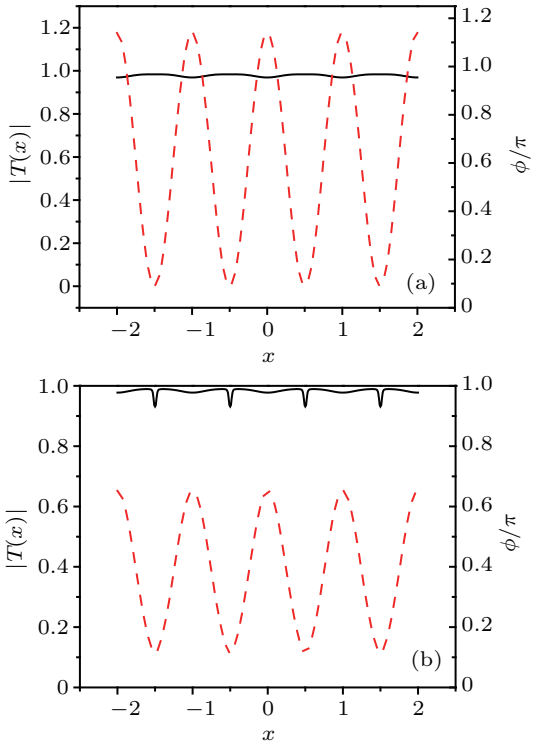


Fig. 2. (color online) The amplitude (solid curves) and phase (dashed curves) of the transmission function $T(x)$ as a function of x. (a) $T = 0$ K, $\Delta_s = 250\gamma$; (b) $T = 300$ K, $\Delta_s = 330\gamma$. The other parameters are $\Omega_c = 15\gamma$, $\Omega_s = 15\gamma$, $\Delta_p = 0.9\gamma$, $\Delta_c = 0$, $\Omega_p = 0.01\gamma$, $L = 920$, $M = 5$, $\Lambda/\lambda_p = 4$, $\gamma_{31} = \gamma_{32} = \gamma_{42} = \gamma$, $\gamma_{21} = \gamma_{43} = \gamma_{41} = 0.004\gamma$, and $\Gamma_{31} = \Gamma_{32} = \Gamma_{42} = 0.66\gamma$.

Figure 3 shows the diffraction pattern as a function of $\sin\theta$. By adjusting the parameters, we can see from Fig. 3(a) that, when $T = 0$ K, with only the amplitude modulation (dashed curve), 97% of the incident field energy is concentrated in the zero-order diffraction direction, and there is almost no energy in the high-order diffraction direction. When adding the phase modulation (solid curve), more energy is transferred to the high-order diffraction direction. The diffraction efficiency of the first-order diffraction direction of the probe beam can reach 34%, while the diffraction efficiency of the zero-order diffraction direction reduces to 9%. In Fig. 3(b), when $T = 300$ K, it has the same rules as that in Fig. 3(a) ($T = 0$ K). The diffraction efficiency of the first-order diffraction direction of probe beam can reach 31%, while the diffraction efficiency of the zero-order diffraction direction is 17%.

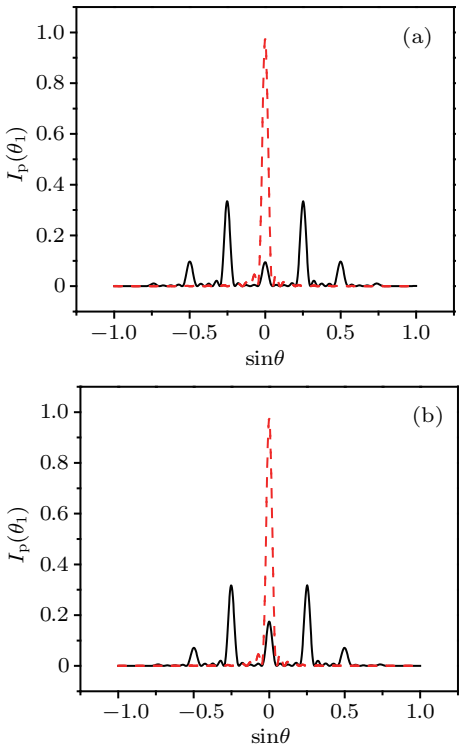


Fig. 3. (color online) The diffraction pattern as a function of $\sin\theta$ with (solid curves) and without (dashed curves) phase modulation. (a) $T = 0$ K, $\Delta_s = 250\gamma$; (b) $T = 300$ K, $\Delta_s = 330\gamma$. Other parameters are the same as those in Fig. 2.

In Figs. 4–6, the first-order diffraction intensities $I_p(\theta_1)$ as a function of Ω_c and Ω_s with different L are given with the temperature changing, respectively. It can be seen when $T = 0$ K (Fig. 4), namely in the cold atomic system, under the condition that other parameters are the same, with the increase of L, the first-order diffraction efficiency of the probe beam is also increased. When $L = 920$, the first-order diffraction efficiency of the probe beam can reach the highest to 34.44%. With the further increase of L, the first-order diffraction efficiency is gradually decreased. At the same time, with the increase of L, the maximum value of the first-order diffraction in each figure corresponding to the relationship between Ω_c and Ω_s is gradually changed from $\Omega_c < \Omega_s$ to $\Omega_c > \Omega_s$. When $T = 100$ K (Fig. 5) and $T = 300$ K (Fig. 6), which are in the thermal atomic system, we found that the first-order diffraction efficiency of the probe beam has the same rules as that in $T = 0$ K (Fig. 4).

From Fig. 4, we can see that the influence of the change of L is very small for the first-order diffraction efficiency of the probe beam (diffraction efficiency from 31% to 34.4%), and from Figs. 5 and 6, the influence of the change of the L on the first-order diffraction efficiency is relatively large (for example, when $T = 100$ K, the first-order diffraction efficiency is only 6% with $L = 45$, however the first-order diffraction efficiency is 27% when $L = 300$).

In Fig. 7, the first-order diffraction intensity $I_p(\theta_1)$ as a function of Δ_p and Δ_s with different T is given. In Fig. 7(a),

when $T = 0$ K, we can see that with the increase of Δ_s, the first-order diffraction efficiency of probe beam is also increased. When $\Delta_s = 245\gamma$, the first-order diffraction efficiency can reach the highest value of 33.6%. With the further increase of Δ_s, the diffraction efficiency decreases gradually, but Δ_p will have little influence on the diffraction intensity of the probe beam. Here, $\Delta_c = 0$, $\Omega_c = 15\gamma$, $\Omega_p = 0.01\gamma$, $\Omega_s = 15\gamma$, $L = 920$, $M = 5$, and $\Lambda/\lambda_p = 4$. When $T = 100$ K or 300 K (other parameters are the same as those at $T = 0$ K), the first-order diffraction efficiency of probe beam increases at first and then decreases with Δ_s increasing. In Figs. 7(b)–7(d), namely in thermal atomic system, Δ_p has also little effect on the first-order diffraction intensity of the probe beam with $\Delta_p < 2\gamma$. However, under the condition of $2\gamma < \Delta_p < 5\gamma$ holding, the first-order diffraction efficiency of the probe beam closes to zero rapidly.

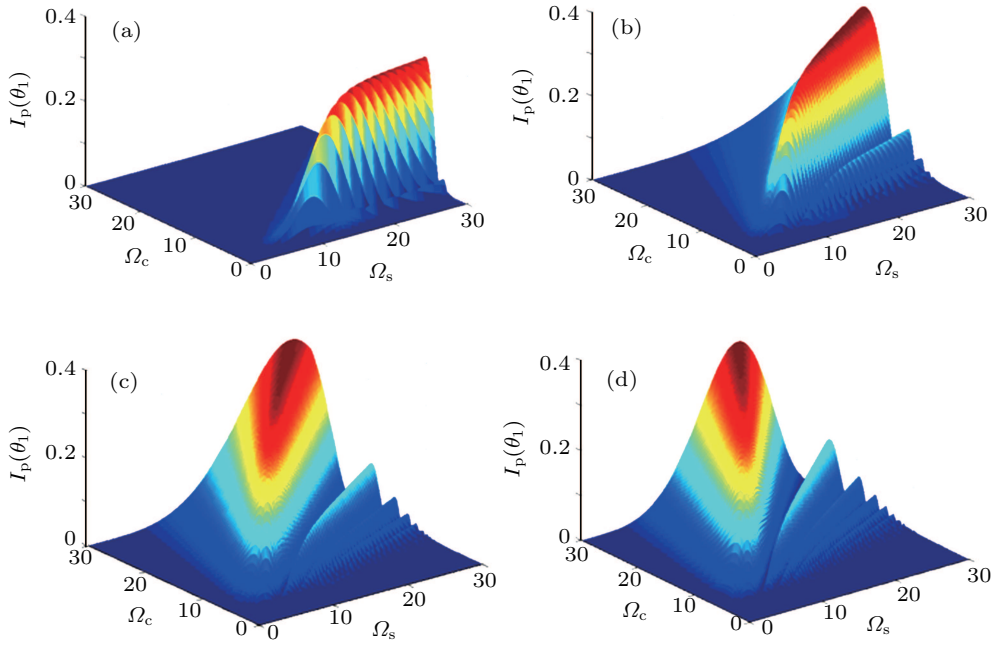


Fig. 4. (color online) First-order diffraction intensity $I_p(\theta_1)$ as a function of Ω_c and Ω_s with different L: (a) $L = 45$; (b) $L = 300$; (c) $L = 920$; (d) $L = 1500$. Here, $\Delta_c = 0$, $\Delta_P = 0.9\gamma$, $\Delta_s = 205\gamma$, $T = 0$ K. Other parameters are the same as those in Fig. 2.

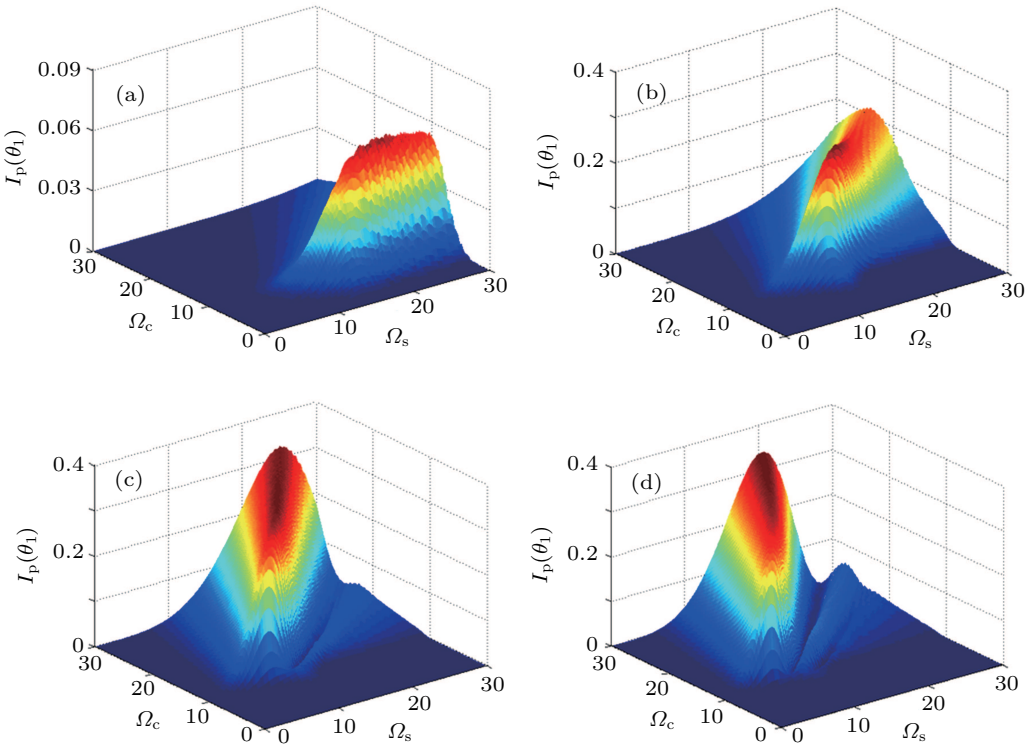


Fig. 5. (color online) First-order diffraction intensity $I_p(\theta_1)$ as a function of Ω_c and Ω_s with different L: (a) $L = 45$; (b) $L = 300$; (c) $L = 920$; (d) $L = 1500$. Here, $T = 100$ K. Other parameters are the same as those in Fig. 4.

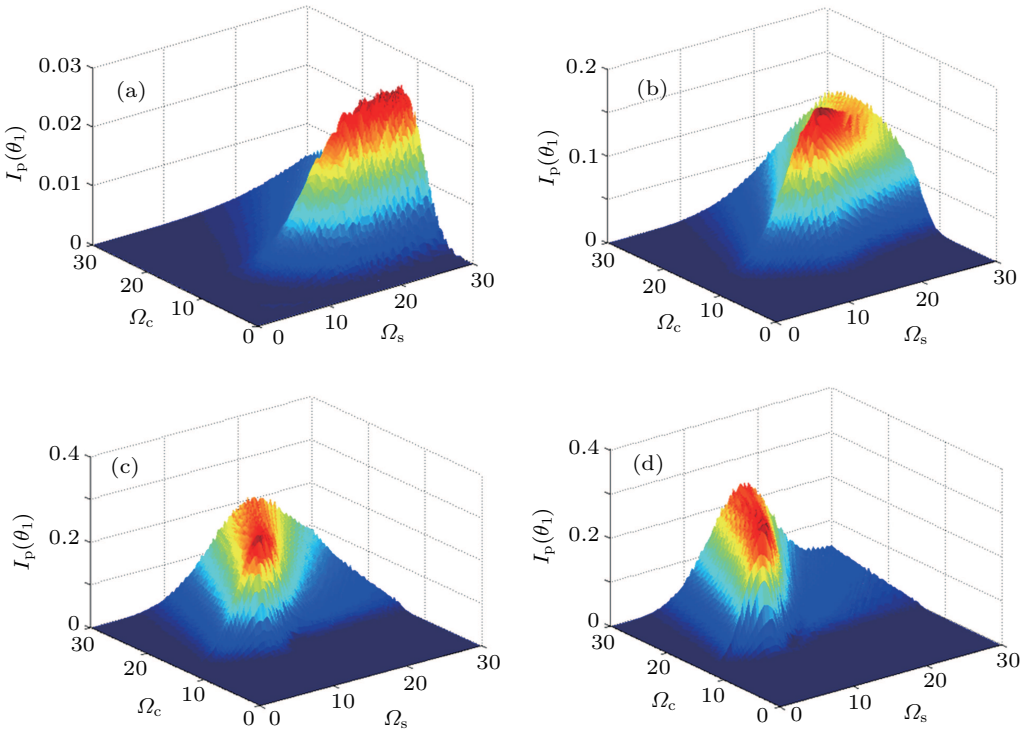


Fig. 6. (color online) First-order diffraction intensity $I_p(\theta_1)$ as a function of Ω_c and Ω_s with different L. (a) $L = 45$; (b) $L = 300$; (c) $L = 920$; (d) $L = 1500$. Here, $T = 300$ K. Other parameters are the same as those in Fig. 4.

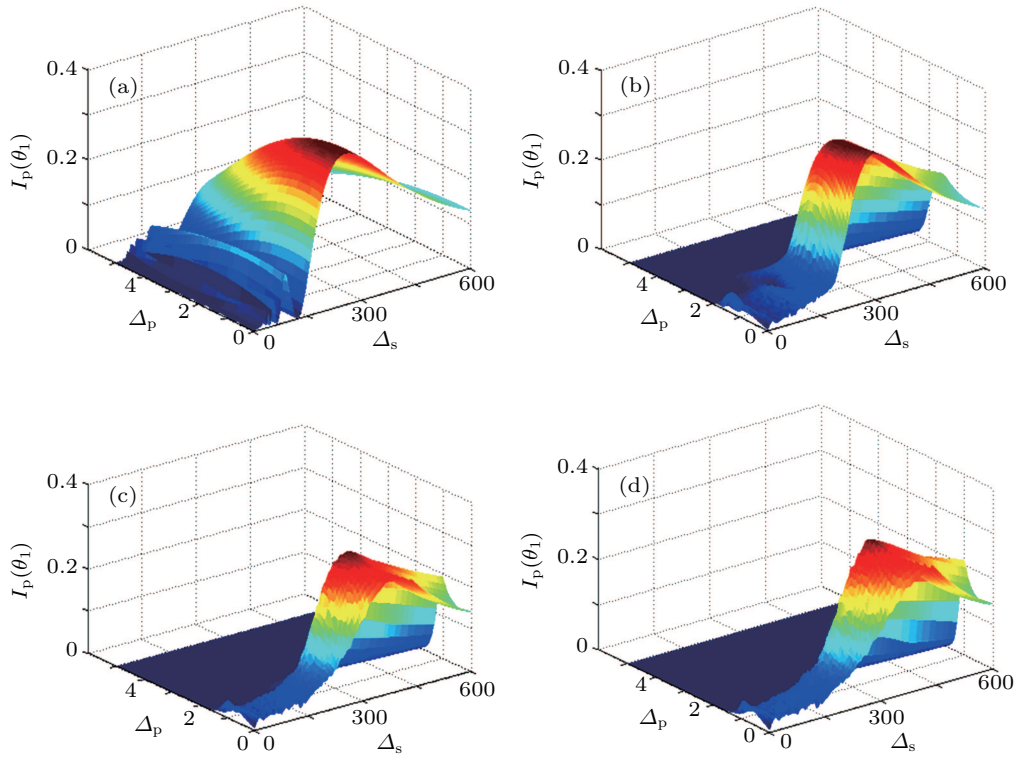


Fig. 7. (color online) First-order diffraction intensity $I_p(\theta_1)$ as a function of Δ_p and Δ_s with different T: (a) $T = 0$ K; (b) $T = 100$ K; (c) $T = 300$ K; (d) $T = 400$ K. Other parameters are the same as those in Fig. 2.

In addition, we can also see from Figs. 4–7 that with the increase of T, the maximum value of the first-order diffraction intensity of the probe beam is reduced gradually.

4. Conclusion

In this paper, we analyzed and compared the factors that may affect the first-order diffraction efficiency of the probe

beam in the thermal atomic system and cold atomic system, and then obtained the laws of the influence on the first-order diffraction efficiency, so that through adjusting parameters, the first-order diffraction efficiency can reach 34% and 31% in the cold atomic system and thermal atomic system, respectively. However, it is more difficult to prepare a cold atomic system than to prepare a thermal atomic system in practical applications. Compared with that in the cold atomic system, the EIG effect in the thermal atomic system may have some advantages in practical applications.

This study also shows that, in order to achieve higher diffraction efficiency, large frequency detuning of the signal field is necessary both in the thermal atomic system and the cold atomic system.

References

[1] Boller K J, Imamoglu A and Harris S E 1991 *Phys. Rev. Lett.* **66** 2593
[2] Gea-Banacloche J, Li Y Q, Jin S and Xiao M 1995 *Phys. Rev. A* **51** 576
[3] Ling H Y, Li Y Q and Xiao M 1998 *Phys. Rev. A* **57** 1338
[4] Dutta B K and Mahapatra P K 2006 *J. Phys. B* **39** 1145
[5] Xiao Z H, Shin S G and Kim K 2010 *J. Phys. B* **43** 161004
[6] Brown A W and Xiao M 2005 *Opt. Lett.* **30** 699
[7] Schilke A, Zimmermann C and Guerin W 2012 *Phys. Rev. A* **86** 023809
[8] Mitsunaga M and Imoto N 1999 *Phys. Rev. A* **59** 4773
[9] Cardoso G C and Tabosa J W R 2002 *Phys. Rev. A* **65** 033803
[10] Zhang Y P, Utsab K, Blake A and Xiao M 2009 *Phys. Rev. Lett.* **102** 013601
[11] Zhang Y P, Wang Z G, Nie Z Q, Li C B, Chen H X, Lu K Q and Xiao M 2011 *Phys. Rev. Lett.* **106** 093904
[12] Zhang Y P, Yuan C Z, Zhang Y Q, Zheng H B, Chen H X, Li C B and Wang Z G 2013 *Laser Phys. Lett.* **10** 055406
[13] de Araujo L E E 2010 *Opt. Lett.* **35** 977
[14] Dong Y B and Guo Y H 2014 *Chin. Phys. B* **23** 074204
[15] Dong Y B, Dong Y E and Gao J R 2008 *Chin. Phys. B* **17** 3306
[16] Dong Y B, Zhang J X, Wang H H and Gao J R 2006 *Chin. Phys.* **15** 1262
[17] Dong Y B, Zhang J X, Wang H H and Gao J R 2006 *J. Phys. B: At. Mol. Opt. Phys.* **39** 3447
[18] Zhao Y T, Zhao J M, Xiao L T, Yin W B and Jia S T 2004 *Chin. Phys. Lett.* **21** 76
[19] Dong Y B, Wang H H, Gao J R and Zhang J X 2006 *Phys. Rev. A* **74** 063810
[20] Xiao Z H, Shin S G and Kim K 2010 *J. Phys. B: At. Mol. Opt. Phys.* **43** 161004
[21] Radu B 1975 *Equilibrium and Non-Equilibrium Statistical Mechanics* (New York: Wiley)